THE JOURNAL OF PHYSICAL CHEMISTRY C

Article

pubs.acs.org/JPCC

Microsphere Light-Scattering Layer Assembled by ZnO Nanosheets for the Construction of High Efficiency (>5%) Quantum Dots Sensitized Solar Cells

Jianjun Tian,*[,†] Lili Lv,[†] Xuyang Wang,[†] Chengbin Fei,[‡] Xiaoguang Liu,[†] Zhenxuan Zhao,[‡] Yajie Wang,[‡] and Guozhong Cao*[,‡,§]

[†]Advanced Materials Technology Institute, University of Science and Technology Beijing, Beijing, 100083, China

[‡]Beijing Institute of Nanoenergy and Nanosystems, Chinese Academy of Sciences, Beijing, 100083, China

[§]Department of Materials Science and Engineering, University of Washington, Seattle, Washington 98195, United States

ABSTRACT: This work reported on a bilayer photoelectrode constructed by ZnO nanoparticle (NP) film and ZnO microsphere (MS) scattering layer for CdS/CdSe quantum dot cosensitized solar cells (QDSCs) with a power conversion efficiency (PCE) of greater than 5%. We controlled the growth orientations of ZnO crystals to form nanosheets, which attached together and assembled into MS due to the high surface energy of the nanosheets. MSs were used as a top layer to effectively increase the light diffuse reflection and harvesting to enhance photogenerated current. In comparison with ZnO NPs photoelectrode, the short circuit current density (J_{sc}) of ZnO NPs/MSs photoelectrode increased from 10.3 mA/cm^2 to 16.0 mA/cm^2, which was an enhancement of 55%. To further increase the fill factor and PCE of QDSCs, ZnO NPs/MSs was treated in the solution of H_3BO_3 and $(NH_4)_2TiF_6$ to form a barrier surface layer, which suppressed the charge recombination and prolonged electron lifetime. As a result, the solar cell displayed J_{sc} of 17.13 mA/cm^2, V_{oc} of 0.56 V, FF of 0.53, and PCE of 5.08%, one of the highest values for ZnO-based QDSCs at this time.

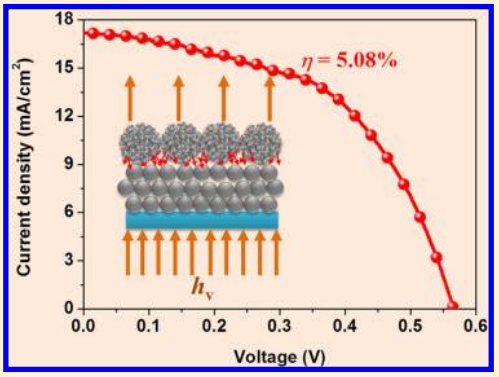

1. INTRODUCTION

The establishment of low cost and high performance solar cells for sustainable energy sources to replace fossil fuels has become an urgent subject imposed on scientists around the world.[1,2] As a cost-effective alternative to silicon-based photovoltaics, quantum dot sensitized solar cells (QDSCs) have attracted considerable attention recently and showed promising development for next generation solar cells.[2−6] QDSCs can be regarded as a derivative of dye-sensitized solar cells (DSCs), which were first reported by O'Regan and Grätzel in 1991.[7] However, QDSCs use semiconductor quantum dots (QDs)[8−11] as the photosensitizer instead of organic dyes because of their versatile optical and electrical properties, such as (1) tunable band gap depending on QD size, (2) larger extinction coefficient, (3) high stability toward water and oxygen, and (4) generation of multiple excitons with single-photon absorption.[12−14] The theoretical photovoltaic conversion efficiency of a QDSC can reach up to 44% in view of the multiple exciton generation (MEG) of QDs.[14,15] Among the various QDs that are used for QDSCs, CdS, and CdSe are attractive owing to their high potential for light harvesting in the visible light region.[12,16] CdSe has a band gap of 1.7 eV and may therefore absorb photons with wavelengths shorter than 700 nm, and shows better performance when compared to CdS. CdS has usually been used to induce CdS/CdSe cosensitization, which broadens the optical absorption of QDs. So far, CdS/CdSe cosensitized QDSCs with TiO_2 electrodes have reached power conversion efficiencies (PCE) higher than 5%.[3,17,18]

Porous nanoparticle films, such as TiO_2 and ZnO, are commonly used for the photoelectrode of QDSCs. However, the small size of the nanoparticles makes the porous films transparent to visible light, which weakens the light harvesting. Recently, the light scattering layer on the surface of the film has been adopted as an effective means to improve the light harvesting of photoelectrodes.[19] In fact, the light scattering layer can cause optical reflection or diffusion to extend the traveling distance of incident light within a photoelectrode film. The enhancement of light scattering on QDSCs can be realized through the use of either a bilayer structure consisting of a light scattering layer over a nanocrystalline film, or a binary combination composed of a nanocrystalline film mixed with submicrometer-sized particles. Various types of light scattering layer, such as photonic crystals and different large-sized metal oxide spheres, have been introduced to increase the absorption path-length of photons, create confinement properties to enhance light harvesting and decrease the probability of charge recombination.[20]

Special Issue: Michael Grätzel Festschrift

Received: December 21, 2013
Revised: February 26, 2014
Published: February 26, 2014

   dx.doi.org/10.1021/jp412525k | J. Phys. Chem. C 2014, 118, 16611−16617

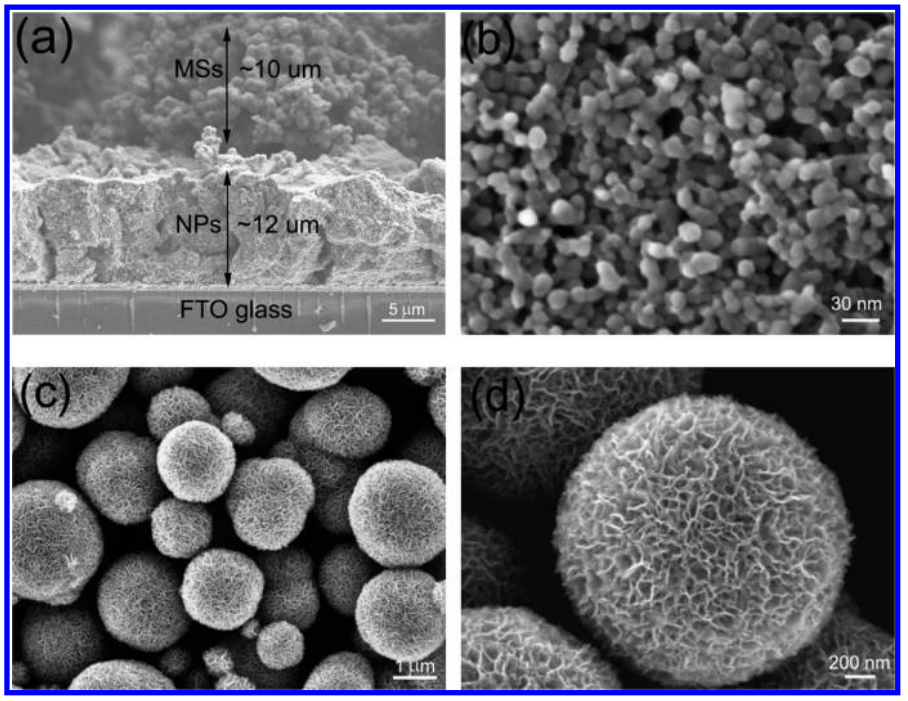

Figure 1. SEM images of (a) the bilayer structure composed of ZnO NPs film and MSs layer, (b) ZnO NPs with size of 20−30 nm, (c, d) low and high magnification of ZnO MSs.

In comparison with TiO_2, ZnO has higher electron mobility, making it an ideal photoelectrode material for QDSCs.[21−23] However, the PCE of ZnO-based QDSCs is still lower than that of TiO_2-based devices due to the high surface charge recombination in ZnO.[24] The high surface charge recombination can be attributed to many defects on ZnO surface, which ultimately boosts the surface charge recombination. In addition, the chemical stability of ZnO is less than that of TiO_2, which makes it easy for ZnO to react with the electrolyte. The instability also decreases the performance of QDSC.[25] Tian and Cao et al.[26] developed a facile modification method for ZnO mesoporous photoelectrode. This method not only opened the apertures to improve the distribution of QDs in the photoeletrode, increased the specific surface area and reduced the surface defects of ZnO photoelectrodes to accommodate more QDs, but also suppressed the charge recombination and prolonged electron lifetime by introducing a barrier layer.

In this work, we designed a light-scattering layer of ZnO microsphere (MS) with assembled nanosheets for the first time. MSs have larger surface area and high diffuse reflection effect to enhance the light capture of the photoelectrode based on ZnO nanoparticles. After that, the ZnO photoelectrodes were immersed in an aqueous solution containing 0.1 M H_3BO_3 and 0.04 M $(NH_4)_2TiF_6$ for the surface modification to suppress the surface charge recombination. As a result, the CdS/CdSe quantum dot sensitized solar cells based on such photoelectrodes displayed a high PCE of 5.08%.

2. EXPERIMENTAL PROCEDURES

2.1. Preparation of ZnO Nanoparticles Film and Microspheres Layer. ZnO nanoparticles with the size of 20−30 nm were prepared by a facile precipitation method. A 0.06 M KOH aqueous solution was gradually added into 0.03 M zinc acetate methanol solution at 60 °C for 60 min, and then were centrifuged and dried at 70 °C. ZnO nanoparticles, ethyl cellulose, and α-terpineol were mixed to paste with weight proportion of 20, 10, and 70%, respectively. The paste was then coated on a fluorine-doped tin oxide (FTO) glass substrate via doctor blading method to get mesoporous films. The as-received ZnO films underwent a sintering process at 480 °C for 30 min. The ZnO nanoparticle films were immersed in an aqueous solution of 0.01 M zinc nitrate, 0.01 M hexamethylenetetramine (HMT) and 0.001 M trisodium citrate at 70 °C for 10 h. The films were drained from the reaction solution and then calcined at 350 °C for 30 min. As for the surface modification process, the films were treated in the aqueous solution of 0.1 M H_3BO_3 and 0.04 M $(NH_4)_2TiF_6$ at room temperature for 30 min. After that, the films were drained from the reaction solution and washed several times by deionized water. Then the modified films were calcined at 400 °C for 30 min.

2.2. Fabrication of CdS/CdSe Sensitized Solar Cells. For the growth of CdS quantum dots, the films were first immersed in a 0.1 M cadmium nitrate ($Cd(NO_3)_2$) methanol solution for 1 min. Successively, the films were dipped into a 0.1 M sodium sulfide (Na_2S) methanol solution for another 1 min to allow S^{2-} to react with the preadsorbed Cd^{2+}, leading to the formation of CdS. This procedure was denoted as one SILAR cycle. In total, five SILAR cycles were employed to obtain a suitable amount of CdS on the TiO_2 film. In a subsequent step, CdSe was deposited on the CdS-coated substrates through a chemical bath deposition (CBD) method. In brief, 0.1 M sodium selenosulfate (Na_2SeSO_3), 0.1 M cadmium acetate $Cd(CH_2COO)_2$, and 0.2 M trisodium salt of nitrilotriacetic acid ($N(CH_2COONa)_3$) were mixed together with a 1:1:1 volume ratio. The CdS-coated substrates were then vertically immersed into the solution for the deposition of the CdSe layer under dark condition at 24 °C for 3 h. After CdSe deposition, a ZnS passivation layer was deposited with two SILAR cycles by soaking the substrate in an aqueous solution containing 0.1 M zinc nitrate and 0.1 M sodium sulfide, which acted as Zn^{2+} and S^{2-} sources, respectively. The electrolyte

dx.doi.org/10.1021/jp412525k | J. Phys. Chem. C 2014, 118, 16611−16617

employed in this study was composed of 1 M S and 1 M Na_2S in deionized water. The counterelectrode was a Cu_2S film fabricated on brass foil. The preparation of the Cu_2S electrode can be described as follows: brass foil was immersed in 37% HCl at 70 °C for 5 min, then rinsed with water and dried in air. Following this step, the etched brass foil was dipped into 1 M S and 1 M Na_2S aqueous solution, resulting in a black Cu_2S layer forming on the foil.

2.3. Characterization. The morphology of the samples was characterized by scanning electron (SEM, JSM-7000) and transmission electron (TEM, Tecnai G2 F20) microscopy. The photovoltaic properties were measured using a CHI electrochemical workstation under AM 1.5 simulated sunlight with a power density of 100 mW/cm^2. Optical absorption (Shimadzu 3600 UV/vis/IR spectrometer) was used to study the light absorption properties of the samples. Electrochemical impedance spectroscopy (EIS) was carried out using a CHI electrochemical workstation to investigate the electronic and ionic processes in the QDSCs.

3. RESULTS AND DISCUSSION

Figure 1a shows the SEM image of the bilayer structured photoelectrode constructed by a bottom film with the thickness of ~12 μm and the top layer with the thickness of ~10 μm. The bottom film is a layer of ZnO nanoparticles (NPs) with the diameter size of 20−30 nm as shown in Figure 1b. The mesoporous ZnO NPs film serves as QDs scaffold to collect and transfer the excited electrons from QDs. ZnO NPs are synthesized through hydrolyzing the ZnO colloid in methanol solution. The methanol not only provided the medium for the reactions, but also acted as ligands to help to grow equiaxial crystals and control the particle size.[27] The top of the photoelectrode is a ZnO microspheres (MSs)-based scattering layer, which enhances the light reflectance to harvest more light absorption. Figure 1c,d display that the ZnO MSs are assembled by nanosheets with the size of ~10 nm in thickness and ~200 nm in length. This hierarchical structure has large surface area, which is helpful for getting more QDs.

Figure 2 shows the XRD spectra of the ZnO NPs film and ZnO NPs film coated with MSs layer on top. The XRD peaks

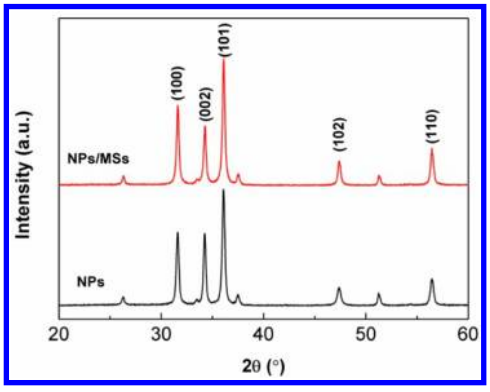

Figure 2. XRD patterns of ZnO NPs and ZnO NPs coated with MSs scattering layer.

can be well indexed to those of standard ZnO (JCPDS 36−1451). As for ZnO NPs, the peak intensity of (100) is approximately equal to that of (002). After the ZnO MSs light scattering layer is applied, the peak intensity of (100) is obviously more than that of (002), which indicates the exposure of (100) crystal facet in MSs is more than that of (002) facet. The possible reason is that ZnO crystals are prone to grow along the ⟨100⟩ orientations during the synthesis of ZnO MSs. To prove the deduction, the formation process of ZnO MSs should are under further study.

Figure 3a,b show the TEM and HRTEM images of the ZnO MSs, respectively, revealing that the ZnO MSs are assembled by

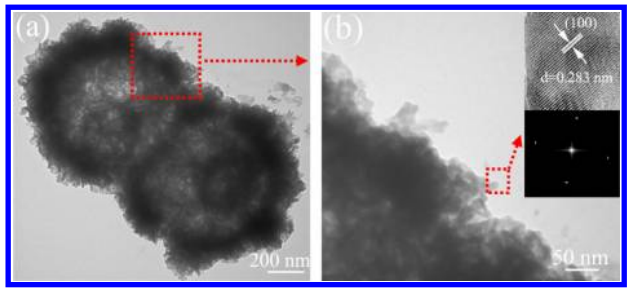

Figure 3. Low resolution (a) and high resolution (b) TEM images of ZnO microspheres of assembled nanosheets, inset showing HRTEM image and fast Fourier transform (FFT) diffraction pattern of ZnO nanosheet.

nanosheets with the size of ~5 nm in thickness and ~50 nm in length. As displayed in Figure 3b and the corresponding inset, the lattice constant and FFT diffraction pattern demonstrate that the nanosheet exhibits a single crystalline structure with (100) facet predominant, indicating that the fastest growth direction for ZnO nanosheet crystal is ⟨100⟩ orientations during the synthesis process. Although the synthesis mechanism of the MSs is not entirely clear, a schematic of the proposed formation mechanism of MSs and nanosheet is illustrated in Figure 4. It has been proposed that HMT reacts

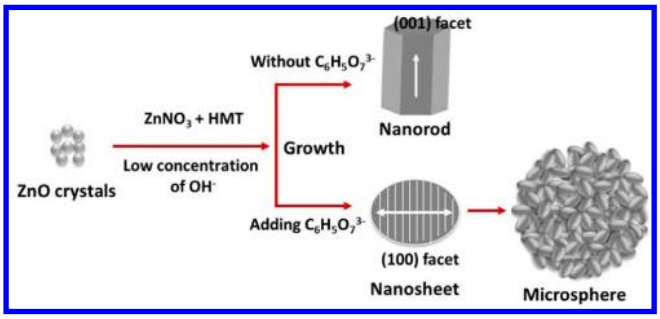

Figure 4. Schematic illustration of ZnO microspheres formation process.

with water to produce ammonia, which in turn reacts with water to generate OH^-.[28,29] HMT can keep a low supersaturation reaction environment of reacting Zn^{2+} with OH^- for ZnO crystals. The chemistry of the process is summarized as follows:[30]

$$C_6H_{12}N_4 + 6H_2O \rightarrow 6CH_2O + 4NH_3 \quad (1)$$

$$NH_3 + H_2O \rightarrow NH_4^+ + OH^- \quad (2)$$

$$Zn^{2+} + 4OH^- \rightarrow Zn(OH)_4^{2-} \quad (3)$$

$$Zn(OH)_4^{2-} \rightarrow Zn(OH)_2 + 2OH^- \quad (4)$$

$$Zn(OH)_2 \rightarrow ZnO + 2H_2O \quad (5)$$

dx.doi.org/10.1021/jp412525k | J. Phys. Chem. C 2014, 118, 16611−16617

Previous research[30,31] showed that ZnO crystals grew fast along the *c*-axis ⟨001⟩ orientation in the low concentration of OH^- ions solution. The growth along *c*-axis was suppressed with the increase of the concentration of OH^- ions. In the reaction solution of $Zn(NO_3)_2$ and HMT, HMT slowly generates OH^- ions. The concentration of OH^- ions always stays at low level. Thus, ZnO crystals grow along ⟨001⟩ orientation to form nanorod. Tian et al.[32] had studied that citrate ions slowed down crystal growth along the ⟨001⟩ orientation, indicating that more citrate ions absorbed on the (001) facet. As displayed in Figure 4, we deduce that citrate ions ($C_6H_5O_7^{3-}$) preferably concentrate on the (001) facet due to its high surface energy, which inhabits the growth of ZnO crystal along ⟨001⟩ orientateon. The crystals are still able to grow sideways (such as ⟨100⟩ orentations) in the form of thin sheets, which is consistent with the results of XRD and TEM. A large numbers of nanosheets would form quickly in the solution and then attach together to form hierarchical structured microspheres due to the high surface energy of the nanosheets.

Figure 5 shows the *J*−*V* curves for the solar cells measured under the illumination of one sun (AM 1.5, 100 mW/cm^{-2}).

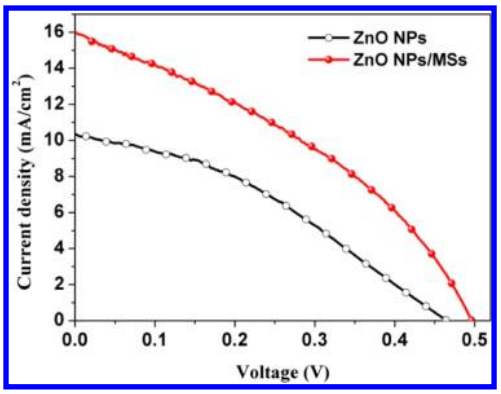

Figure 5. *J*−*V* curves of QDSCs assembled with different photoelectrodes.

The performance parameters, open voltage (V_{oc}), short current density (J_{sc}), fill factor (FF), and PCE of the solar cells are listed in Table 1. In comparison with ZnO NPs photoelectrode,

Table 1. Photovoltaic Properties of QDSCs Assembled with Different Photoelectrodes

photoelectrodes	V_{oc} (V)	J_{sc} (mA/cm^2)	FF	PCE (%)
ZnO NPs	0.46	10.3	0.35	1.66
ZnO NPs/MSs	0.50	16.0	0.36	2.89

J_{sc} of the ZnO NPs/MSs increases from 10.3 to 16.0 mA/cm^2, which is an enhancement of 55%. So the light scattering is an important cause for the increase of the absorbance of incident photons for the enhancement of photogenerated current. Diffuse reflectance and transmittance data can reveal the extent to which incident light is scattered by particles in the photoelectrodes and how much the incident light passes through the photoelectrodes without being scattered.[33] The ideal light scattering properties of a photoanode should be a high diffuse reflectance and low diffuse transmission. Figure 6a,b shows the diffuse reflection and transmittance spectra curves of ZnO photoelectrodes films. It can be seen that the diffuse reflectance of ZnO NPs/MSs is much stronger than that of ZnO NPs in the 400−800 nm range, which is the main wavelength range for QDs to capture photons. In addition, the diffuse transmittance of the ZnO NPs/MSs is much weaker than that of NPs film, which indicates there are more photons trapped in the NPs/MSs film. Figure 6c shows the effect of light scattering layer on the ZnO photoelecrodes. The results can be attributed to the strong scattering of the MSs, which makes the incident light directly reflect back toward the nanoparticles. As a result, the photocurrent and PCE of the QDSC assembled with ZnO NPs/MSs are increased due to the enhanced light scattering.

Although the J_{sc} of QDSCs can be increased by scattering layer, the FF and PCE are still low. The main cause is attribute to the high surface charge recombination due to many defects on the surface of ZnO.[24] In order to decrease the defects and enhance efficiency of QDSCs, the ZnO photoelectrodes were treated by a facile passivation process. The ZnO NPs/MSs films were immersed in an aqueous solution containing 0.1 M H_3BO_3 and 0.04 M $(NH_4)_2TiF_6$ at room temperature for 30 min. The films were then washed several times with deionized water and annealed at 400 °C (detailed information shown in our previous research[26]). Such treatment leads to the formation of a thin passivation layer on the surface of the ZnO NPs/MSs. The modification process can be expressed via the following equations:[26,34]

$$TiF_6^{2-} + 2H_2O \leftrightarrow TiO_2 + 6F^- + 4H^+ \quad (6)$$

$$H_3BO_3 + 4H^+ + 4F^- \leftrightarrow BF_4^- + H_3O^+ + 2H_2O \quad (7)$$

$$ZnO + 2H_3O \rightarrow^+ Zn^{2+} + 3H_2O \quad (8)$$

The reactions 6 and 7 can be shifted to the right by reaction 8, which indicates the dissolution of ZnO can boost the hydrolization of TiF_6^{2-}. With the dissolution of ZnO, TiO_2 nanoparticles are directly deposited on the fresh surface of ZnO. Figure 7a,b show SEM images of the modified ZnO MSs. It can be seen that MSs appear tarnished, and the edge of nanosheets loses keenness and become mellow. As shown in Figure 7c,d, energy-dispersive X-ray spectroscopy (EDS) mapping images of Zn and Ti elements show the presence of Ti elements on the surface of modified ZnO MSs, which indicates ZnO MSs are coated with TiO_2.

To evaluate the effect of surface modification on the resistance distribution and charge recombination, electrochemical impedance spectroscopy (EIS) measurements were carried out. Figure 8a,b shows the impedance spectra of the QDSCs measured under the dark condition with forward bias of −0.6 V. In Figure 8a, the semicircle represents the electron transfer at the photoelectrode/QDs/electrolyte interface and the transport in the photoelectrode (R_{ct}).[35] The R_{ct} of the modified ZnO NPs/MSs based QDSC is 57.2 Ω, which is more than twice of the ZnO NPs/MSs device (22.7 Ω). The charge transfer resistance at the photoelectrode/electrolyte interface (R_{ct}) is determined by both the ZnO and TiO_2 passivation layer, and the total charge transfer resistance can be written by the following eq 9:[36]

$$R_{total} = R_{ZnO} + R_{TiO_2} \quad (9)$$

where R_{ZnO} and R_{TiO_2} are the electron transfer resistances induced by the ZnO and TiO_2 passivation layer, respectively. EIS results indicate that electrons in the ZnO photoelectrode with passivation layer are more difficult to recombine with holes in the electrolyte in view of its high R_{ct}. R_{ct} can be

dx.doi.org/10.1021/jp412525k | J. Phys. Chem. C 2014, 118, 16611−16617

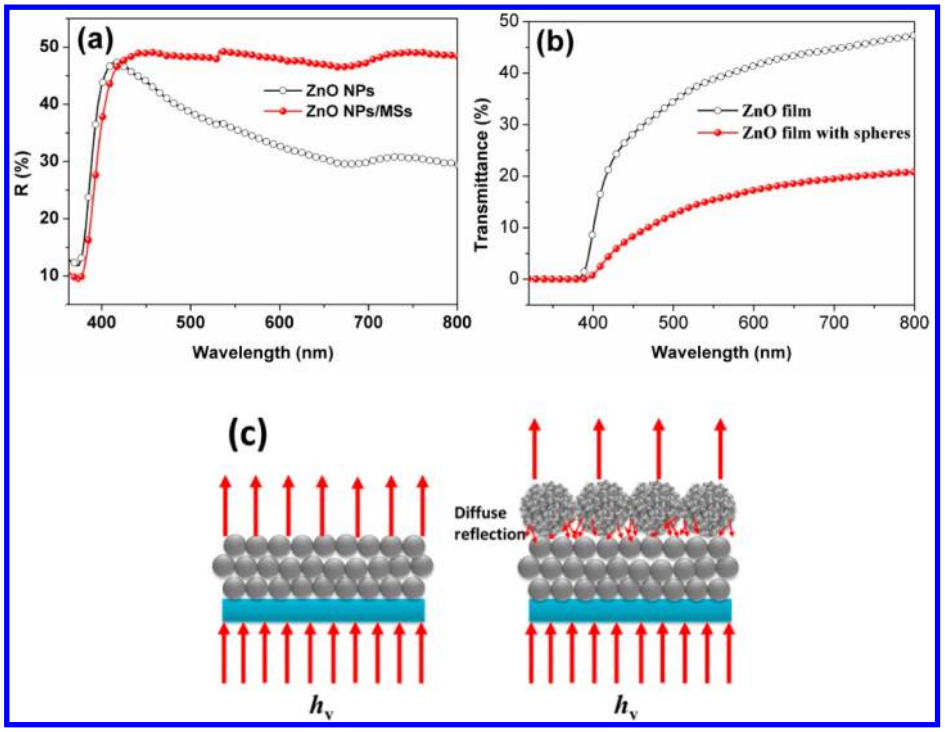

Figure 6. Diffuse reflection (a), transmittance spectra curves (b) of ZnO films and (c) schematic illustration of the effect of light scattering layer on the ZnO films.

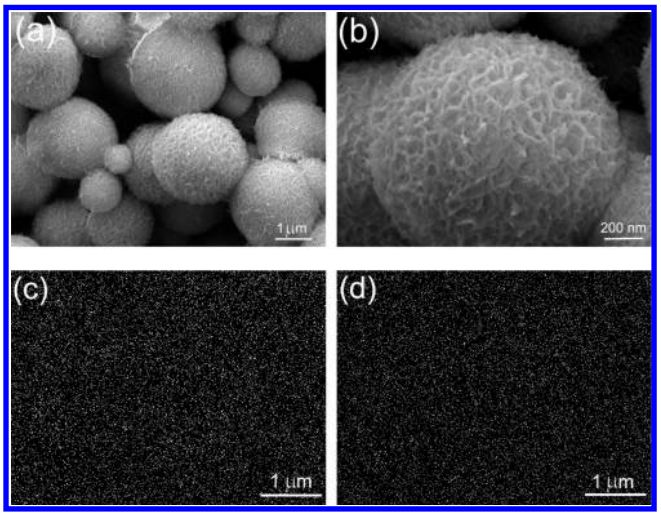

Figure 7. Low resolution (a) and high resolution (b) SEM images of modified ZnO microspheres, and elements distribution mapping images of (c) Zn and (d) Ti.

considered as part of a shunt resistance (R_{sh}) because it behaves like a diode on the applied bias voltage.[36] The R_{sh} relates to the FF according to the following eq 10:[36]

$$FF = FF_0(1 - 1/R_{sh}) \quad (10)$$

where FF_0 is the theoretical maximum FF. It can be inferred that the increase in FF of the QDSC assembled with the modified photoelectrode is a result of an increase in R_{sh}. Figure 8b shows the bode plots of the QDSCs with the different photoelectrodes. The curve peak of the spectrum can be used to determine the electron lifetime in the ZnO (according to the equation $\tau_n = 1/(2\pi f_{min})$).[37] It is clear that the electron lifetime for the device with the modified ZnO NPs/MSs photoelectrode is 11.6 ms, which is much longer than the 4.2 ms of electron lifetime for the ZnO NPs/MSs. The electron lifetime (τ_n) is directly proportional to R_{ct} and is calculated by eq 11:[38]

$$\tau_n = R_{ct} \cdot C_\mu \quad (11)$$

where C_μ is the corresponding chemical capacitance. Consequently, the employment of modified TiO_2 layer can enhance the charge recombination resistance and thus prolong the electron lifetime.[36,39] Figure 8c shows the schematic illustration surface charge recombination pathways of QDSC: (A) recombination of electrons in the QD conduction band and holes in the QD valence band; (B) recombination of electrons with the electron acceptors in the electrolyte; (C) back electron injection from ZnO to electrolyte; (D) back electron injection from ZnO to QDs. Among these pathways, processes (A) and (B) can be ignored due to the highly efficient charge separation.[24] Recombination pathways (C) and (D) can be considered as the main factors that affect the performance of a QDSC. The recombination depends on photelectrode/QDs/electrolyte interfacial resistance. As a barrier layer, the TiO_2 modification layer can increase the interfacial resistance to reduce recombination.[26] So, the FF and PCE of QDSCs will be increased evidently by the modification treatment.

Figure 9 shows the $J-V$ curves for the solar cells measured under the illumination of one sun (AM 1.5, 100 mW cm^{-2}). Detailed results of the samples are shown in Table 2. Compared with ZnO NPs based QDSC, the FF and PCE of the modified ZnO NPs/MSs based QDSCs increased from 0.36 to 0.53 and 2.89 to 5.08%, respectively. To our knowledge, the PCE of 5.08% is one of the highest respective values for ZnO-based QDSCs at this time.

4. CONCLUSIONS

A bilayer structured photoelectrode of ZnO nanoparticle (NP) film and ZnO microsphere (MS) scattering layer for CdS/CdSe

dx.doi.org/10.1021/jp412525k | J. Phys. Chem. C 2014, 118, 16611−16617

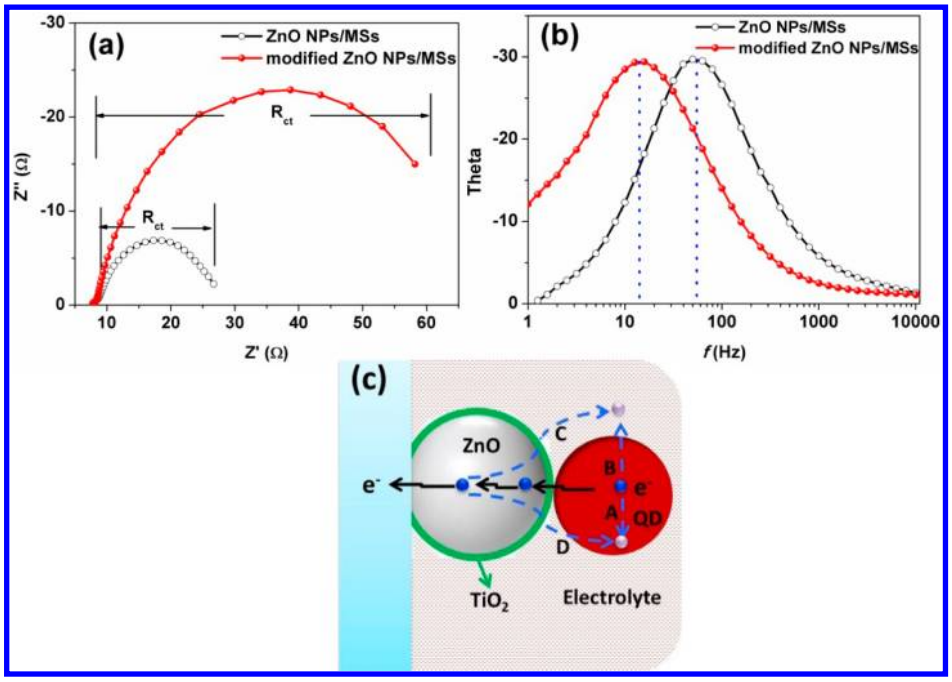

Figure 8. (a) Nyquist plots curves and (b) bode plot curves of the QDSCs under forward bias (−0.6 V) and dark condition, and (c) schematic illustration of the surface charge recombination pathways of QDSC.

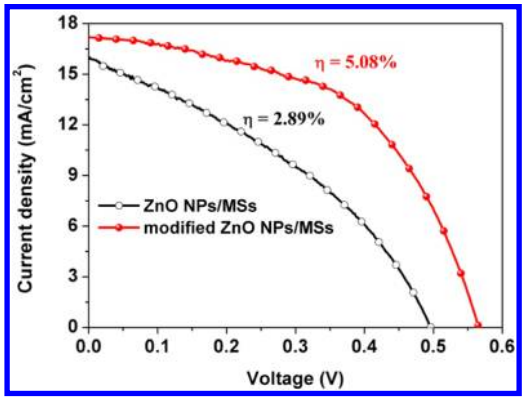

Figure 9. *J*–*V* curves of QDSCs with different photoelectrodes.

Table 2. Photovoltaic Properties of QDSCs with Different Photoelectrodes

photoelectrodes	V_{oc} (V)	J_{sc} (mA/cm^2)	FF	PCE (%)
ZnO NPs/MSs	0.50	16.01	0.36	2.89
modified ZnO NPs/MSs	0.56	17.13	0.53	5.08

quantum dot cosensitized solar cells (QDSCs) was examined in this investigation. The MS layer could effectively increase the light diffuse reflection and harvesting to enhance photogenerated current. However, the FF and PCE of QDSC were still low due to the high surface charge recombination. ZnO NPs/MSs was treated in the solution of H_3BO_3 and $(NH_4)_2TiF_6$ to form a thin barrier layer on its surface, which suppressed the charge recombination and prolonged electron lifetime. As a result, the solar cell displayed a high performance, J_{sc} of 17.13 mA/cm^2, V_{oc} of 0.56 V, FF of 0.53, and PCE of 5.08%, which was one of the highest respective values for ZnO-based QDSCs at this time.

AUTHOR INFORMATION

Corresponding Authors

*E-mail: tianjianjun@mater.ustb.edu.cn.
*E-mail: gzcao@u.washington.edu.

Notes

The authors declare no competing financial interest.

ACKNOWLEDGMENTS

This work was supported by the National Science Foundation of China (51374029 and 51174247) and Program for New Century Excellent Talents in University (NCET-13-0668) and the Fundamental Research Funds for the Central Universities (FRF-TP-12-153A).

REFERENCES

(1) Grätzel, M.; Janssen, R. A. J.; Mitzi, D. B.; Sargent, E. H. Materials Interface Engineering for Solution-Processed Photovoltaics. *Nature* **2012**, *488*, 304−312.
(2) Tada, H.; Fujishima, M.; Kobayashi, H. Photodeposition of Metal Sulfide Quantum Dots on Titanium(IV) Dioxide and the Applications to Solar Energy Conversion. *Chem. Soc. Rev.* **2011**, *40*, 4232−4243.
(3) Santra, P. K.; Kamat, P. V. Mn-Doped Quantum Dot Sensitized Solar Cells: A Strategy to Boost Efficiency Over 5%. *J. Am. Chem. Soc.* **2012**, *134*, 2508−2511.
(4) Hossain, M. A.; Jennings, J. R.; Koh, Z. Y.; Wang, Q. Carrier Generation and Collection in CdS/CdSe-Sensitized SnO_2 Solar Cells Exhibiting Unprecedented Photocurrent Densities. *ACS Nano* **2011**, *5*, 3172−3181.
(5) Ryu, J.; Lee, S. H.; Nam, D. H.; Park, C. B. Rational Design and Engineering of Quantum-Dot-Sensitized TiO_2 Nanotube Arrays for Artificial Photosynthesis. *Adv. Mater.* **2011**, *23*, 1883−1888.
(6) Sugaya, T.; Numakami, O.; Oshima, R.; Furue, S.; Komaki, H.; Amano, T.; Matsubara, K.; Okano, Y.; Niki, S. Ultra-High Stacks of InGaAs/GaAs Quantum Dots for High Efficiency Solar Cells. S. *Energy Environ. Sci.* **2012**, *5*, 6233−6237.
(7) Oregan, B.; Gratzel, M. A Low-Cost, High-Efficiency Solar-Cell Based on Dye-Sensitized Colloidal TiO_2 Films. *Nature* **1991**, *353*, 737−740.

(8) Bang, J. H.; Kamat, P. V. Solar Cells by Design: Photoelectrochemistry of TiO_2 Nanorod Arrays Decorated with CdSe. *Adv. Funct. Mater.* **2010**, *20*, 1970−1976.
(9) Gonzalez-Pedro, V.; Xu, X.; Mora-Sero, I.; Bisquert, J. Modeling High-Efficiency Quantum Dot Sensitized Solar Cells. *ACS Nano* **2010**, *4*, 5783−5790.
(10) Yu, X. Y.; Liao, J. Y.; Qiu, K. Q.; Kuang, D. B.; Su, C. Y. Dynamic Study of Highly Efficient CdS/CdSe Quantum Dot-Sensitized Solar Cells Fabricated by Electrodeposition. *ACS Nano* **2011**, *5*, 9494−9500.
(11) Cheng, C. W.; Karuturi, S. K.; Liu, L. J.; Liu, J. P.; Li, H. X.; Su, L. T.; Tok, A. I. Y.; Fan, H. J. Quantum-Dot-Sensitized TiO_2 Inverse Opals for Photoelectrochemical Hydrogen Generation. *Small* **2012**, *8*, 37−42.
(12) Zhu, G.; Pan, L.; Xu, T.; Sun, Z. CdS/CdSe-Cosensitized TiO_2 Photoanode for Quantum-Dot-Sensitized Solar Cells by a Microwave-Assisted Chemical Bath Deposition Method. *ACS Appl. Mater. Interfaces* **2011**, *3*, 3146−3151.
(13) Lee, Y. L.; Lo, Y. S. Highly Efficient Quantum-Dot-Sensitized Solar Cell Based on Co-Sensitization of CdS/CdSe. *Adv. Funct. Mater.* **2009**, *19*, 604−609.
(14) Tian, J. J.; Gao, R.; Zhang, Q. F.; Zhang, S. G.; Li, Y. W.; Lan, J. L.; Qu, X. H.; Cao, G. Z. Enhanced Performance of CdS/CdSe Quantum Dot Cosensitized Solar Cells via Homogeneous Distribution of Quantum Dots in TiO_2 Film. *J. Phys. Chem. C* **2012**, *116*, 18655−18662.
(15) Li, T. L.; Lee, Y. L.; Teng, H. High-Performance Quantum Dot-Sensitized Solar Cells Based on Sensitization with $CuInS_2$ Quantum Dots/CdS Heterostructure. *Energy Environ. Sci.* **2012**, *5*, 5315−5324.
(16) Lee, Y. H.; Im, S. H.; Chang, J. A.; Lee, J. H.; Seok, S. I. CdSe-Sensitized Inorganic-Organic Heterojunction Solar Cells: The Effect of Molecular Dipole Interface Modification and Surface Passivation. *Org. Electron.* **2012**, *13*, 975−979.
(17) Hossain, M. A.; Jennings, J. R.; Shen, C.; Pan, J. H.; Koh, Z. Y.; Mathews, N.; Wang, Q. CdSe-Sensitized Mesoscopic TiO_2 Solar Cells Exhibiting >5% Efficiency: Redundancy of CdS Buffer Layer. *J. Mater. Chem.* **2012**, *22*, 16235−16242.
(18) Pan, Z. X.; Zhang, H.; Cheng, K.; Hou, Y. M.; Hua, J. L.; Zhong, X. H. Highly Efficient Inverted Type-I CdS/CdSe Core/Shell Structure QD-Sensitized Solar Cells. *ACS Nano* **2012**, *6*, 3982−3991.
(19) Wang, W.; Zhang, H.; Wang, R.; Feng, M.; Chen, Y. Design of a TiO_2 Nanosheet/Nanoparticle Gradient Film Photoanode and Its Improved Performance for Dye-Sensitized Solar Cells. *Nanoscale* **2014**, *6*, 2390−2396.
(20) Tian, J. J.; Zhang, Q. F.; Uchaker, E.; Liang, Z. Q.; Gao, R.; Qu, X. H.; Zhang, S. G.; Cao, G. Z. Constructing ZnO Nanorod Array Photoelectrodes for Highly Efficient Quantum Dot Sensitized Solar Cells. *J. Mater. Chem. A* **2013**, *1*, 6770−6775.
(21) Chou, T. P.; Zhang, Q. F.; Fryxell, G. E.; Cao, G. Z. Hierarchically Structured ZnO Film for Dye-Sensitized Solar Cells with Enhanced Energy Conversion Efficiency. *Adv. Mater.* **2007**, *19*, 2588−2592.
(22) Zhang, Q. F.; Cao, G. Z. Hierarchically Structured Photoelectrodes for Dye-Sensitized Solar Cells. *J. Mater. Chem.* **2011**, *21*, 6769−6774.
(23) Zhang, Q. F.; Chou, T. R.; Russo, B.; Jenekhe, S. A.; Cao, G. Z. Aggregation of ZnO Nanocrystallites for High Conversion Efficiency in Dye-Sensitized Solar Cells. *Angew. Chem., Int. Ed.* **2008**, *47*, 2402−2406.
(24) Tian, J. J.; Zhang, Q. F.; Zhang, L. L.; Gao, R.; Shen, L. F.; Zhang, S. G.; Qu, X. H.; Cao, G. Z. ZnO/TiO_2 Nanocable Structured Photoelectrodes for CdS/CdSe Quantum Qot Co-Sensitized Solar Cells. *Nanoscale* **2013**, *5*, 936−943.
(25) Irannejad, A.; Janghorban, K.; Tan, O. K.; Huang, H.; Lim, C. K.; Tan, P. Y.; Fang, X.; Chua, C. S.; Maleksaeedi, S.; Hejazi, S. M. H.; et al. Effect of the TiO_2 Shell Thickness on the Dye-Sensitized Solar Cells with ZnO-TiO_2 Core-Shell Nanorod Electrodes. *Electrochim. Acta* **2011**, *58*, 19−24.
(26) Tian, J. J.; Zhang, Q. F.; Uchaker, E.; Gao, R.; Qu, X. H.; Zhang, S. G.; Cao, G. Z. Architectured ZnO Photoelectrode for High Efficiency Quantum Dot Sensitized Solar Cells. *Energy Environ. Sci.* **2013**, *6*, 3542−3547.
(27) Sun, D.; Wong, M.; Sun, L.; Li, Y.; Miyatake, N.; Sue, H. J. Purification and Stabilization of Colloidal ZnO Nanoparticles in Methanol. *J. Sol-Gel Sci. Technol.* **2007**, *43*, 237−243.
(28) Dong, H. P.; Wang, L. D.; Gao, R.; Ma, B. B.; Qiu, Y. Constructing Nanorod-Nanoparticles Hierarchical Structure at Low Temperature as Photoanodes for Dye-Sensitized Solar Cells: Combining Relatively Fast Electron Transport and High Dye-Loading Together. *J. Mater. Chem.* **2011**, *21*, 19389−19394.
(29) Wu, C. T.; Liao, W. P.; Wu, J. J. Three-Dimensional ZnO Nanodendrite/Nanoparticle Composite Solar Cells. *J. Mater. Chem.* **2011**, *21*, 2871−2876.
(30) Zhou, Z.; Deng, Y. Kinetics Study of ZnO Nanorod Growth in Solution. *J. Phys. Chem. C* **2009**, *113*, 19853−19858.
(31) Cao, B.; Cai, W. From ZnO Nanorods to Nanoplates: Chemical Bath Deposition Growth and Surface-Related Emissions. *J. Phys. Chem. C* **2008**, *112*, 680−685.
(32) Tian, Z. R. R.; Voigt, J. A.; Liu, J.; McKenzie, B.; McDermott, M. J.; Rodriguez, M. A.; Konishi, H.; Xu, H. F. Complex and Oriented ZnO Nanostructures. *Nat. Mater.* **2003**, *2*, 821−826.
(33) Gao, R.; Tian, J.; Liang, Z.; Zhang, Q.; Wang, L.; Cao, G. Nanorod-Nanosheet Hierarchically Structured ZnO Crystals on Zinc Foil as Flexible Photoanodes for Dye-Sensitized Solar Cells. *Nanoscale* **2013**, *5*, 1894−1901.
(34) Yodyingyong, S.; Zhou, X. Y.; Zhang, Q. F.; Triampo, D.; Xi, J. T.; Park, K.; Limketkai, B.; Cao, G. Z. Enhanced Photovoltaic Performance of Nanostructured Hybrid Solar Cell Using Highly Oriented TiO_2 Nanotubes. *J. Phys. Chem. C* **2010**, *114*, 21851−21855.
(35) Koide, N.; Islam, A.; Chiba, Y.; Han, L. Y. Improvement of Efficiency of Dye-Sensitized Solar Cells Based on Analysis of Equivalent Circuit. *J. Photochem. Photobiol., A* **2006**, *182*, 296−305.
(36) Park, K.; Zhang, Q. F.; Garcia, B. B.; Cao, G. Z. Effect of Annealing Temperature on TiO_2-ZnO Core-Shell Aggregate Photoelectrodes of Dye-Sensitized Solar Cells. *J. Phys. Chem. C* **2011**, *115*, 4927−4934.
(37) Kern, R.; Sastrawan, R.; Ferber, J.; Stangl, R.; Luther, J. Modeling and Interpretation of Electrical Impedance Spectra of Dye Solar Cells Operated Under Open-Circuit Conditions. *Electrochim. Acta* **2002**, *47*, 4213−4225.
(38) Wang, Q.; Ito, S.; Gratzel, M.; Fabregat-Santiago, F.; Mora-Sero, I.; Bisquert, J.; Bessho, T.; Imai, H. Characteristics of High Efficiency Dye-Sensitized Solar Cells. *J. Phys. Chem. B* **2006**, *110*, 25210−25221.
(39) Park, K.; Zhang, Q. F.; Garcia, B. B.; Zhou, X. Y.; Jeong, Y. H.; Cao, G. Z. Effect of an Ultrathin TiO_2 Layer Coated on Submicrometer-Sized ZnO Nanocrystallite Aggregates by Atomic Layer Deposition on the Performance of Dye-Sensitized Solar Cells. *Adv. Mater.* **2010**, *22*, 2329−2332.